IL NUOVO CIMENTO Vol. 30 C, N. 3 Maggio-Giugno 2007
DOI 10.1393/ncc/i2007-10241-y

Comparative study of feature classification methods for mass lesion recognition in digitized mammograms

G. L. Masala([1])([*]), S. Tangaro([3])([**]), B. Golosio([1]), P. Oliva([1]), S. Stumbo([1]), R. Bellotti([3]), F. De Carlo([3]), G. Gargano([3]), D. Cascio([2]), F. Fauci([2]), R. Magro([2]), G. Raso([2]), U. Bottigli([5]), A. Chincarini([6]), I. De Mitri([7]), G. De Nunzio([7]), I. Gori([8]), A. Retico([8]), P. Cerello([9]), S. C. Cheran([9]), C. Fulcheri([10]) and E. Lopez Torres([11])

([1]) *Struttura Dipartimentale di Matematica e Fisica dell'Università di Sassari and INFN Sezione di Cagliari - Cagliari, Italy*
([2]) *Dipartimento di Fisica e Tecnologie Relative dell'Università di Palermo and INFN Sezione di Catania - Catania, Italy*
([3]) *Dipartimento di Fisica dell' Università di Bari and INFN, Sezione di Bari - Bari, Italy*
([4]) *Dipartimento di Fisica dell' Università di Lecce and INFN, Sezione di Lecce - Lecce, Italy*
([5]) *Dipartimento di Fisica dell'Università di Siena and INFN, Sezione di Pisa - Pisa, Italy*
([6]) *Dipartimento di Fisica dell'Università di Genova and INFN, Sezione di Genova Genova, Italy*
([7]) *Dipartimento di Fisica dell' Università di Lecce and INFN, Sezione di Lecce - Lecce, Italy*
([8]) *INFN, Sezione di Pisa - Pisa, Italy*
([9]) *INFN, Sezione di Torino - Torino, Italy*
([10]) *Dipartimento di Fisica dell'Università di Torino - Torino, Italy*
([11]) *CEADEN - Havana, Cuba*

(ricevuto il 12 Giugno 2007; revisionato il 27 Luglio 2007; approvato il 31 Luglio 2007; pubblicato online il 18 Ottobre 2007)

Summary. — In this work a comparison of different classification methods for the identification of mass lesions in digitized mammograms is performed. These methods, used in order to develop Computer Aided Detection (CAD) systems, have been implemented in the framework of the MAGIC-5 Collaboration. The system for identification of mass lesions is based on a three-step procedure: a) preprocessing and segmentation, b) region of interest (ROI) searching, c) feature extraction and classification. It was tested on a very large mammographic database (3369 mammographic images from 967 patients). Each ROI is characterized by eight features extracted from a co-occurrence matrix containing spatial statistics information on the ROI pixel grey tones.

([*]) E-mail: giovanni.masala@ca.infn.it
([**]) E-mail: sonia.tangaro@ba.infn.it

The reduction of false-positive cases is performed using a classification system. The classification systems we compared are: Multi Layer Perceptron (MLP), Probabilistic Neural Network (PNN), Radial Basis Function Network (RBF) and K-Nearest Neighbours classifiers (KNN). The results in terms of sensitivity (percentage of pathological ROIs correctly classified) and specificity (percentage of non-pathological ROIs correctly classified) are presented. MLP and RBF outperform other classification algorithms by about 8% of the area under the ROC curve.

PACS 87.57.Ra – Computer-aided diagnosis.
PACS 87.58.Mj – Digital imaging.
PACS 87.57.Nk – Image analysis.
PACS 87.59.Ek – Mammography.

1. – Introduction

The increasing development of decision systems in medical environments has highlighted the need to explore more effective architectures for mining and representing data. Among emblematic cases there is breast cancer. In Italy cancer of the breast represents a quarter of the total women's tumours and it affects about three thousand women every year. The living women struck down with this disease are about three hundred thousand while only 10% of people in jeopardy are currently subjected to a breast screening. Also, it is generally known that women regularly subjected to screening have a statistically significant reduction of mortality for cancer of the breast compared to women not subjected to screening [1]. Besides, the double independent of mammogram reading executed by two radiologists improves the sensibility of mammogram screening [2, 3] of the 4–15% of the number of revealed cancers. A computer-assisted analysis of this screening data would be a time and cost effective way to help radiologists to detect tumors as early as possible.

Within the MAGIC-5 (Medical Application on a Grid Infrastructure Connection) project, a collaboration among Italian physicists and radiologists, a large database of digitized mammographic images was built and used to develop a CAD (Computer Aided Diagnosis) tool for the automated detection of lesions in mammographic images. MAGIC-5 has developed an integrated station that is used to digitize analogical images, archive them in DICOM format and to perform their statistical analysis. Furthermore this prototype of station can represent a very good system for mammographic educational programs: with a GRID configuration it is possible for the clinicians to tele- and co-work in new and innovative groupings [4]. Using the whole database, several analysis can be performed with the MAGIC-5 tools.

The mammographic images ($18 \times 24\,\mathrm{cm}^2$, digitized by a CCD linear scanner with a $85\,\mu$m pitch, 4096 grey levels and 12 bit depth) are fully characterized: the pathological ones have a consistent description which includes the radiological diagnosis and the histological data; the non-pathological ones correspond to patients with a follow-up of at least three years [5]. This work focuses on the automated search for and analysis of masses usually characterized by peculiar shapes. The ROI characterization is made by extracting the Haralik set of features [6]. The choice for texture-based features is justified by the successful applications of such features to the detection of pathologies in medical image analysis [7, 8].

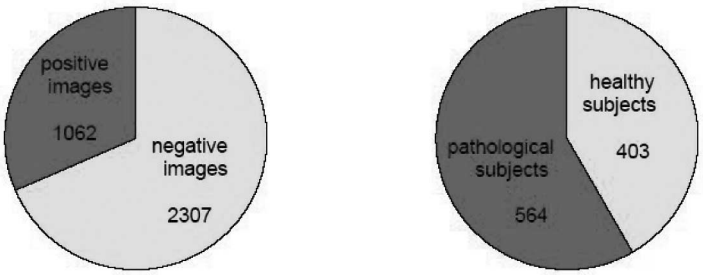

Fig. 1. – Database composition: images (left) and subjects (right).

We discuss the results obtained in the reduction of false-positive cases with different classifiers: a Feed Forward Neural Network, a K-Nearest Neighbours [9-11] approach. In this work a comparison is made with respect to own previous work [12] where we used different features on the same dataset of ROIs.

2. – Materials and methods

The Database [5, 12, 13] used to train and test the classifications methods was acquired in various mammographic centers using different mammographic screen/film systems and settings (all with molybdenum anode). It is composed of 3369 anonymized mammographic images, each including data and clinical information, collected from 967 patients. There are 1601 (48%), 1456 (43%) and 312 (9%) cranio caudal/oblique/lateral views, respectively. The image size is 2067×2657 pixels, the pitch $85\,\mu$m, the dynamic range 12 bits/pixel (4096 grey levels). All the mammographic images were collected in the Italian hospitals involved in the project from 1997 to 2002.

All the images containing one (or more) lesions were characterized according to the kind of lesions (mass or microcalcification cluster), the grade of malignancy, the kind of breast texture, etc.

In the database there are images from 306 (32%) *normal* patients (with no evidence

Legend	
IRO	Irregular Roundish Opacity
SO	Spiculated Opacity
RRO	Regular Roundish Opacity
PS	Parenchymal Distorsion
BRO	Blurred Roundish Opacity

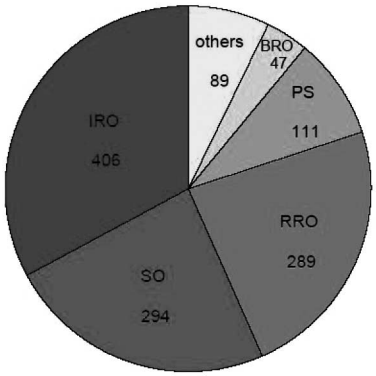

Fig. 2. – Different kinds of masses present in the database.

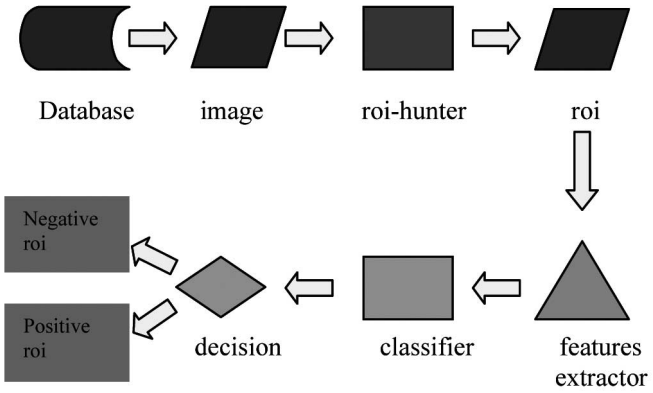

Fig. 3. – Block diagram. The ROI-hunter selects the regions of interest from the analyzed images. Each ROI is characterized by some features extracted from the co-occurrence matrix. A classifier is used to distinguish the pathological patterns from the healthy ones.

of any lesion after a three years radiological follow-up) and from 661 (68%) *abnormal* patients. Due to the fact that this study is focused on the detection of masses, disregarding other mammographic pathologies as microcalcification, we consider pathological only abnormal subjects with massive lesions. Consequently, the positive images are the ones containing at least one mass, as diagnosed by an expert radiologist and confirmed by biopsy; images with no mass at the first exam and after a follow-up of at least three years are considered as negative, even if they contain some other pathology. Hence, the breakdown of the cases, due to the previously reported definition of *positive*, is displayed in fig. 1 for both the images and the analyzed subjects. For many malignant lesions cytological and/or histological results are also available. The database contains 1062 images with at least one mass and 304 images with at least one cluster of microcalcifications. The total number of lesions is 1620 (1236 masses and 384 microcalcification clusters). A pie diagram summarising the statistics of the different kinds of masses in the database is shown in fig. 2.

The CAD system presented here is based on main three steps: a ROI-hunter, a features extractor module and a classifier, as shown in fig. 3. In the following sections each of the above-mentioned processing step is described in detail.

2˙1. *Segmentation methods.* – The Regions Of Interest (ROI) hunter should allow to focus only on the suspicious areas of the mammogram, thus reducing the amount of data to be processed, without lost of relevant information. To this purpose, three main requests should be satisfied by the segmentation algorithm:

– The efficiency, defined as the fraction of detected masses with respect to the ones diagnosed by the radiologist, should be as close as possible to 1. This is a fundamental parameter of the analysis as undetected lesions at the segmentation level are definitively missed.

– The number of false positives per image (FPpI) should be as low as possible: a high number of ROIs found in each image leads to many undesired false alarm regions submitted to the radiologist's examination.

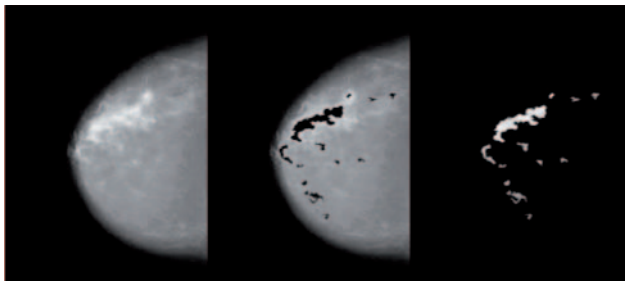

Fig. 4. – The original mammogram (left), the remaining image (middle), the selected patterns containing the ROIs (right).

– The ROI area percentage should be as small as possible, in order to fit the mass at best, thus reducing the computational burden.

A detailed description of the ROI hunter, including the parameter selection, is given in [14, 12]. Here we briefly provide the main points the algorithm is based on:

– the mammogram is divided into square cells of 200×200 pixels and a relative grey level maximum I_{m} (initial center for the candidate lesion) is searched in each cell;

– an iso-intensity contour, defining a ROI with area A_{R} which includes the relative maximum intensity pixel, is drawn for a certain initial threshold value value $I_{\mathrm{th}} = I_{\mathrm{m}}/2$;

– the threshold is increased/decreased provided that the ROI area A_{R} is greater/smaller than a limit area $A_{\max}$; the iteration is stopped when the difference between two consecutive thresholds is equal to one;

– the ROI is removed and stored for feature extraction and classification;

– the processing is repeated for the following square cell.

Only selected regions are stored for the next processing steps, as shown in fig. 4.

The number of ROIs detected from each image is not set *a priori*, rather it is related to the texture properties of the mammogram. All the ROIs extracted from negative

TABLE I. – *Composition of the mammographic dataset: The central column represents the total number of ROIs used (positive and negative) while the right column represents only the pathological (positive) ROIs.*

	Dataset	
Dataset	No. of samples (ROIs)	No. of positive samples (ROIs)
Training set	4230	318
Validation set	4230	315
Testing set	4230	320

TABLE II. – *Composition of train, test or validation set.*

Subset composition	
Number of ROIs	type of ROIs
1793	healthy ROIs from healthy image
2104	healthy ROIs from positive image
182	Positive ROIs - close constraint to overlap
151	Positive ROIs - weak constraint to overlap
4230	Tot

images are tagged as negatives, while the ROIs from positive images can be labeled as true positive (TP) if they overlap with the contours of the medical diagnosis, otherwise as false positive (FP). Also, in same images the masses could not be perfectly centred by ROI-hunter. A close constraint to overlap is that the distance of the ROI center from the real mass center is minor than the real radius of the mass (we consider as real mass the medical diagnosis). While a weaker constraint (in this case the ROI have the additional noise) is that the center of the mass is included into the ROI. In the used subset, tables I and II, the differences between healthy ROI extracted from healthy images and healthy ROI extracted from positive images are also considered.

2˙2. *The features extractor module.* – The focus of the analysis is the computation of the Grey Level Co-occurrence Matrix (GLCM) [6], also known as Spatial Grey Level Dependence (SGLD). To this purpose, we consider the minimal rectangular portion of the image which fully includes the ROI. As the name suggests, the GLCM is constructed from the image by estimating the pairwise statistics of pixel intensity, thus relying on the assumption that the texture content information of an image is contained in overall or average spatial relationship between pairs of pixel intensities [6]. A co-occurrence matrix M is a $G \times G$ matrix, whose rows and columns are indexed by the image grey levels $i = 1, \ldots, G$, where $G = 2^n$ for a n-bit image. Each p_{ij} element represents an estimate of the probability that two pixels with a specified polar separation d, θ have grey levels i and j. The d and θ coordinates are the distance and the angle between the two pixels i and j, respectively. In their seminal paper, Haralik *et al.* [6] considered only $d = 1$ displacements at quantized angles ($\theta = k\pi/4$, with $k = 0, 1, 2, 3$), thus having

$$M_{d,\theta}(j, i) = M_{d,\theta+\pi}(j, i).$$

Symmetry is achieved by averaging the GLCM with its transpose, thus leading to invariance under π rotations too. Textural features can be derived from the GLCM and used in texture classification, replacing the single GLCM elements. A number of 14 features is introduced, related to textural properties of the image such as homogeneity, contrast, presence of organized structures, complexity and nature of grey tone transitions. The values of these features are sensitive to the choice of the direction θ, since the parameter d is set to 1. Invariance under rotation should be restored in order to avoid describing two images, one obtained by rotating the other, with different feature sets. This is achieved by considering the average and range of each feature values over the

θ angles, thus obtaining a number of 28 textural variables. Some of them are used as inputs to the classifier [13, 15].

As the texture is grey tone independent, either the image must be normalized or one should choose features which are invariant under monotonic grey level transformations. As previously pointed out, the images of our database come from different centers and no kind of normalization is applied. For this reason we select, among all the GLCM features, the ones that are invariant under monotonic grey tone transformation:

– energy

$$f_1 = \sum_{ij} p_{ij}^2 \,;$$

– entropy

$$f_2 = -\sum_{ij} p_{ij} \ln(p_{ij});$$

– information measures of correlation:

$$f_3 = \frac{f_2 - H_1}{\max\{H_x, H_y\}},$$
$$f_4 = [1 - \exp[-2(H_2 - f_2)]]^{1/2} \,,$$

where

$$P_x(i) = \sum_j p_{ij} \,,$$
$$P_y(j) = \sum_i p_{ij} \,,$$
$$H_1 = -\sum_{ij} p_{ij} \ln\{P_x(i)P_y(j)\} \,,$$
$$H_2 = -\sum_{ij} P_x(i)P_y(j) \ln\{P_x(i)P_y(j)\} \,.$$

For each of the above-mentioned features, the average and range are computed for the $\theta = k\pi/4$ angles, with $k = 0, 1, 2, 3$, and $d = 1$, thus obtaining eight textural features.

It turns out that using the average and variance of the extracted indices is more efficient with respect to the use of the not mediated features. In fact our previous studies with these not mediated features have supplied poor results.

Table I shows the composition of the training, validation and testing sets. The first column represents the total number of ROIs (positive and negative) in the sample, while the second column represents only the pathological (positive) ROIs.

Some comments concerning the relation of this work with other previous ones [12, 13] are as follows. The database at our disposal is the same as in [12, 13], *i.e.* the CALMA database, but with a different arrangement of the training and test sets (with respect to [13]) and different features (with respect to [12]). In particular, the training phase is

optimized by using a greater number of ROIs in the training phase; in addition the sets are chosen in a way that the proportion of the type of ROIs is preserved, as shown in table II.

A classification has been carried out to discriminate different types of masses with a multiclass problem and the sensitivity of the system does not improve with respect to the two-class problem [16].

A study of the representation space is made with two types of Component Analysis [9]: the Principal Component Analysis (PCA) and the Independent Component Analysis (ICA). The PCA algorithm makes use of the Karhunen Loève transformation [9] to reduce the features with the main eigenvalues of the covariance matrix of the mean vectors.

Although the PCA algorithm found the principal component, in our problem the populations of the positive and negative samples remain rather overlapped after the transformation. So the PCA algorithm is not suitable in our classification problem.

While the PCA seeks directions in a features space that best represents the data in a sum-squared error sense [9], the ICA seeks directions that are most independent of each other. In particular a Fast Independent Component Analysis (FASTICA) is used to provide a computationally quick method to estimate the unobserved independent components [17]. It is a method to decompose a multi-dimensional dataset into a set of statistically independent non-Gaussian variables. The algorithm iteratively maximises an approximation to the negentropy of the projected data [17]. The negentropy is based on the information-theoretic quantity of entropy which measures the "randomness" of an observed variable. Since Gaussian variables have the largest entropy among all random variables of equal variance, entropy can be used to define a measure of non-Gaussianity (*i.e.* negentropy). Typical algorithms for ICA use centering, whitening and dimensionality reduction as pre-processing steps in order to simplify and reduce the complexity of the problem for the actual iterative algorithm. By using FASTICA on the same dataset we optimised the algorithm with a preliminary features reduction through Whitening method [9]. Then the independent components are found by optimizing FASTICA parameters [17]: however, with this approach also the positive and negative samples remain rather overlapped after the transformation.

2˙3. *The classifier.* – We made a comparative study of three different neural networks, a deterministic classifier and a classifier that implements an optimal evolution of the theory of linear discriminative functions. We discuss here the results obtained with the following classifiers:

- Multi Layer Perceptron (MLP). In this classifier the units each perform a biased weighted sum of their inputs and pass this activation level through a transfer function to produce their output, and the units are arranged in a layered feed forward topology. The network thus has a simple interpretation as a form of input-output model, with the weights and thresholds (biases) the free parameters of the model. The selected MLP is a feed-forward back-propagation supervised neural network trained with gradient a descent learning rule with "momentum".
- Probabilistic Neural Network (PNN). In the PNN, there are at least three layers: input, radial, and output layers. The radial units are copied directly from the training data, one per case. Each models a Gaussian function centered at the training case. There is one output unit per class. Each is connected to all the radial units belonging to its class, with zero connections from all other radial units.

Hence, the output units simply add up the responses of the units belonging to their own class. The outputs are each proportional to the kernel-based estimates of the probability density function of the various classes, and by normalizing these to sum to 1.0 estimates of class probability are produced.

– Radial Basis Function (RBF) network with a static Gaussian function. This classifier has a hidden layer of radial units, each actually modeling a Gaussian response surface. Since these functions are nonlinear, it is not actually necessary to have more than one hidden layer to model any shape of function: sufficient radial units will always be enough to model any function. A linear combination of the outputs (*i.e.* a weighted sum of the Gaussians) is made to model any nonlinear function. The standard RBF has an output layer containing dot product units with identity activation function.

– K-Nearest Neighbors (K-NN) classifier. It is amongst the simplest of all machine learning algorithms. An object is classified by a majority vote of its neighbors, with the object being assigned the class most common amongst its k nearest neighbors. k is a positive integer, typically small. If $k = 1$, then the object is simply assigned the class of its nearest neighbor. In binary (two class) classification problems, it is helpful to choose k to be an odd number as this avoids difficulties with tied votes. This value of K is often approximately close to $N^{1/2}$.

3. – Results

For each classifier the training and validation sets are used for the optimization and cross validation [9] phases. The test set, in terms of ROIs but with different features representation, is the same of previous studies [12]. The feature reduction through PCA gives the same results with respect to the original dataset but it slightly reduces the computing time. Using FASTICA the performance is bad, so this method is not suitable. In both cases, classifiers on raw data give better performances compared to PCA and FASTICA. This is a strong argument against using component analysis for this dataset.

Using sensitivity (percentage of pathologic ROIs correctly classified) and specificity (percentage of healthy ROIs correctly classified), the results obtained with this analysis are described in terms of the ROC (Receiver Operating Characteristic) curve [18, 19], which shows the true positive fraction (sensitivity), and the false positive fraction (1-specificity) with respect to the threshold level of the ROI selection procedure.

In this way the ROC curve allows the radiologist to detect masses with predictable performance, so that the required CAD sensitivity value can be set before starting a study.

In particular we obtain for the classifiers the following configuration:

– MLP has 13 hidden neurons for the 8 inputs previously described.

– PNN gives the best performance with a 0.072 spread parameter.

– RBF has 65 neurons in the radial layer with a 2.5 spread parameter.

– KNN is optimized for $K = 49$ on the validation set; an additional threshold set allows to generate the ROC curve.

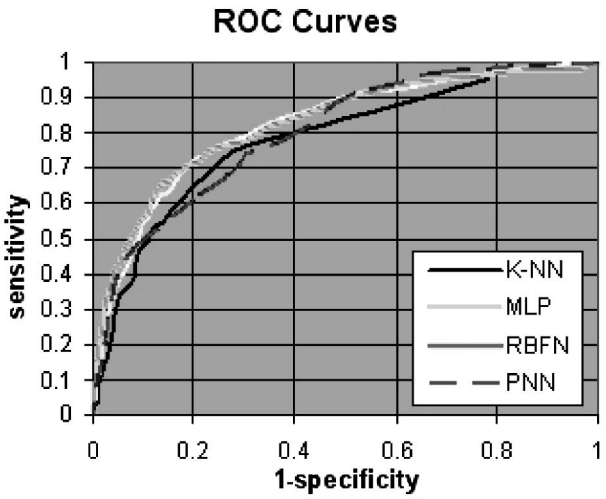

Fig. 5. – Receive Operating Characteristic curves for several classifiers tried on the testing set.

The classifiers results are shown in the diagram in terms of the ROC curve calculated on the testing set after the optimization on the validation set.

Finally in fig. 5 the results of the classifiers on the testing set (on original features space) are shown.

The areas under the curve [18, 19] are reported in table III.

The results (table III) show that the neural networks (RBF, MLP) give better performances than the other classifiers. A study on the complementariness of the classifiers used on the dataset under examination shows (in the case of the features previously used) that the regions of decision of the three classifiers overlap. This fact indicates that it is not possible to combine the output of the various classifiers with techniques of multi classification system (MCS) to improve the global performance.

In table IV the results of the best classifiers on the testing set are compared on original features space, with PCA-representation and FASTICA representation.

So we can conclude that the best data representation in our problem is in the original

TABLE III. – *Performance of the classifiers in terms of Area under the ROC curves on original features spaces.*

Performances of the classifiers		
Classifiers	Area under ROC curves	Error
KNN	0.752	0.017
MLP	0.821	0.015
PNN	0.803	0.015
RBF	0.825	0.014

TABLE IV. – *Performance of the RBF classifiers in terms of Area under the ROC curves in different features spaces.*

Performances of the RBF		
Features spaces	Area under ROC curves	Error
Original data	0.825	0.014
PCA	0.813	0.015
FASTICA	0.651	0.019

features space. In fact using the PCA the results are similar to original features space while the performances with FASTICA are poor.

Also using dissimilarity representation, as described in previous work [16], of this dataset of personal benchmark, the performances of classifiers do not improve with respect to the results shown. In fact in that case the dataset was selected and composed of good ROIs.

So comparing the best results found in this work with the results obtained on the same dataset but with morphological characterization of the features [12] we can conclude that the best approach on mass detection is with neural networks (MLP, PNN, RBF) with morphological features (up 6% of area under ROC curve with respect to these results).

A comparative study of the methods described here and in ref. [12] shows that it is not possible to combine together the outputs of the classifiers with techniques of multi classification systems (MCS) to improve the global performance; in addition it is not suitable to use together morphological features and features extracted from co-occurrence matrix.

4. – Conclusion

A comparison of different algorithms used in a Computer Aided Detection (CAD) system for masses classification has been presented. The CAD system is based on a three-step procedure: a) pre-processing and segmentation, b) region of interest (ROI) search, and c) feature extraction and classification and was tested on a very large mammographic database.

The algorithms classify starting from eight features extracted from a co-occurrence matrix containing second-order spatial statistics information on ROI pixel grey levels.

The algorithms we implemented and tested as classifiers are: Multi Layer Perceptron, Probabilistic Neural Network, Radial Basis Function Network and the K-Nearest Neighbours classifiers.

The best results are obtained with a Radial Basis Function and a Multi Layer Perceptron, which outperform other classification algorithms by about 8% in terms of the area under the ROC curve.

* * *

A part of the results reported in this paper have been produced by the Cybersar project managed from the Cosmolab Consortium. A project partially funded from the Ministero dell'Università e della Ricerca (MIUR) by the Piano Operativo Nazionale

"Ricerca Scientifica, Sviluppo Tecnologico, Alta Formazione" (PON 2000-2006). More information is available on web page: `http://www.cybersar.com`.

REFERENCES

[1] Tabar L. *et al.*, *Lancet*, **1** (1985) 829.
[2] Thrfjell E. L. *et al.*, *Radiology*, **191** (1994) 241.
[3] Warren Burhenne L. J. *et al.*, *Radiology*, **215** (2000) 554.
[4] Cerello P., Bagnasco S., Bottigli U., Delogu P., Fantacci M. E., Fauci F., Forni G., Lauria A., Lopez Torres E., Magro R., Masala G. L., Oliva P., Palmiero R., Ramello L., Raso G., Retico A., Sitta M., Tangaro S. and Zanon E., *Methods Inf. Med.*, **44** (2005) 244.
[5] Lauria A., Massafra R., Tangaro S., Bellotti R., Fantacci M., Delogu P., Lopez Torres E., Cerello P., Fauci F., Magro R. and Bottigli U., *GPCALMA: an Italian mammographic database of digitized images for research, Proceedings of IWDM, Manchester 18-21 June 2006, Lecture Notes in Computer Science*, **4046** (Springer) 2006.
[6] Haralik R. M., Shanmugam K. and Dinstein I., *IEEE Trans. Syst. Man Cybern.*, Vol. SMC-3 11 (1973) 610.
[7] Weszka J. S., Dyer C. R. and Rosenfeld A., *IEEE Trans. Syst. Man Cybern.*, **6** (1976) 269.
[8] Wei D., Chan H.-P., Petrick N., Sahiner B., Helvie M. A., Adler D. D. and Goodsitt M. M., *Med. Phys.*, **24** (1997) 903.
[9] Duda O., Hart P. E. and Stark D. G., "*Pattern Classification*", second edition (A Wiley-Interscience Publication John Wiley & Sons) 2001.
[10] Russel S. J. and Norvig P., "*Artificial Intelligence. A modern approach*" (UTET) 1998.
[11] Haykin S., "*Neural Networks — A comprehensive foundation*", second edition (Prentice Hall) 1999.
[12] Bottigli U., Chiarucci R., Golosio B., Masala G. L., Oliva P., Stumbo S., Cascio D., Fauci F., Glorioso M., Jacomi M., Magro R. and Raso G., *Int. J. Biomed. Sci., ISSN 1306-1216*, **1** (2006) 56.
[13] Bellotti R., De Carlo F., Gargano G., Maggipinto G., Tangaro S., Castellano M., Massafra R., Cascio D., Fauci F., Magro R., Raso G., Lauria A., Forni G., Bagnasco S., Cerello P., Cheran S. C., Lopez Torres E., Bottigli U., Masala G. L., Oliva P., Retico A., Fantacci M. E., Cataldo R., De Mitri I. and De Nunzio G., *Med. Phys.*, **33** (2006) 3066.
[14] Fauci F., Bagnasco S., Bellotti R., Cascio D., Cheran S. C., De Carlo F., De Nunzio G., Fantacci M. E., Forni G., Lauria A., Lopez Torres E., Magro R., Masala G. L., Oliva P., Quarta M., Raso G., Retico A. and Tangaro S., *IEEE Trans. Nucl. Sci. (TNS)*, **5** (2006) 2827.
[15] Conners R. W., Trivedi M. M. and Harlow C. A., *Computer Vision, Graphics and Image Processing*, **25** (1984) 273.
[16] Masala G., Golosio B., Cascio D., Fauci F., Tangaro S., Quarta M., Cheran S. C. and Torres E. L., *Nuovo Cimento C*, **28** (2005) 905.
[17] Aapo Hyv¨arinen and Erkki Oja, *Neural Networks*, **13** (2000) 411.
[18] Hanley J. A. and Mcneil B., *Radiology*, **143** (1982) 29.
[19] Hanley J. A. and Mcneil B., *Radiology*, **148** (1983) 839.